Chapter 4

Thin Manganese films on Si(111)

4.1 Transition metal silicides

The elements with unfilled d- or f-shells exhibit a strong chemical reactivity. For example, they react with silicon to form silicides, stable metal-silicon compounds of various stoichiometries. The deposition of transition metal (TM) atoms onto silicon surfaces is accompanied by a geometric rearrangement and formation of silicides, initially in the contact region and, if supported by sufficient annealing, all over a reacted region, many layers thick. The study of TM thin films on Si is important both for the implications for silicon and silicide technology and for fundamental reasons, since the understanding of the reaction mechanism involved in interface growth in this case is in principle simpler than for compound semiconductors. Nevertheless, the problem remains a difficult one mainly because the interface reaction takes place at temperatures well below the temperature usually needed to form silicides. The discussion of this problem is a prerequisite for any further progress in the understanding of junction formation and thus it has received a great experimental and theoretical effort [34].
From a technological point of view, silicide formation and growth are very important topics because, for example, for microelectronics, micro-sized silicides with low and metal-like resistivity and high temperature stability, are arranged in very-large-scale-integrated (VLSI) circuits, while for optoelectronic devices, semiconductor silicides are used in combination with an in-

direct band gap semiconductor.

Recently, the new field of "spintronics" devices for non-volatile memories brought great attention to the magnetic properties of semiconductors. The prototype device that is already in use in industry as a read head and a memory-storage cell is the giant-magnetoresistive (GMR) sandwich structure which consists of alternating ferromagnetic and non-ferromagnetic metal layers [35]. Depending on the relative orientation of the magnetizations in the metallic layers, the device resistance changes from small (parallel resistance) to large (antiparallel resistance). This change in resistance (generally called magnetoresistance) is used to sense changes in magnetic fields.

In addition, semiconductors may enhance GMR devices with other properties [36]. While metal-based GMR devices do not amplify signals, semiconductor-based spintronics devices could in principle provide amplification and serve, in general, as multi-functional devices, being also much easier for semiconductor-based devices to be integrated with traditional semiconductor technology. For this reason, the recent discovery that GaAs presents ferromagnetic behaviour when doped with manganese, brought a new impetus in studying the structural and electronic properties of such semiconductors, where Mn impurities act, on the one side, as dopants for GaAs semiconductors and, at the same time, introduce the magnetic properties in this semiconductor [37]. Therefore, $Ga_{1-x}Mn_xAs$ has been subject, in the last few years, of many investigations, which led to a good knowledge of many properties of this semiconductor, which is a member of the class of diluted magnetic semiconductors (DMS), composed by III-V semiconductors doped with manganese.

Also different mechanisms for magnetoresistance have been proposed for other materials, and in particular for the intriguing narrow-gap insulator FeSi. This (Kondo) insulator, which already attracted attention for over 30 years because of its anomalous electrical, optical and magnetic properties [38], presents a metal-insulator transition when doped with either Al or Co. More recently it has gained renewed attention because, when doped by substitution of a single species, say Co or Mn, for Fe, it is a low carrier density magnetic metal with exceptional magnetoconductance [39]. In addition, a successive investigation of $Fe_{1-x}Co_xSi$ and $Fe_{1-x}Mn_xSi$ showed a large anomalous Hall effect (AHE) [40], which does not seem to be related to the scattering of Co (or Mn) impurities, but most likely is intrinsic, de-

rived from band structure effects. In this sense (Fe,Co)Si and (Fe,Mn)Si represent a class of materials different from the (III,Mn)V in which the electrons involved in electrical conduction are different from those localized ones responsible for the magnetism, and act as scattering sites for the mobile electrons, such that field tuning of the scattering strength gives rise to the magnetoresistance observed in these materials. In FeSi-based ferromagnets, the magnetoresistance arises from quantum interference effects, and the same electrons are responsible for both magnetic properties and electrical conduction. One more important characteristic of these newly discovered magnetic systems is the complete miscibility of FeSi with CoSi and MnSi (all three have the same cubic B-20 crystal structure), very different from the (Ga,Mn)As system for which the miscibility of Mn is limited by Mn segregation. Therefore, the main problems related to (Ga,Mn)As, i.e. the high defect density and the low compatibility with Si, can be overcome by the introduction of these new systems, although the disadvantage of a lower Curie temperature (T_C) still exists. In fact, the (Ga,Mn)As materials present a high Curie temperature, which, in (III,Mn)V semiconductors, depends on the carrier concentration, and a semiconductor of this class with a T_C of about room temperature has been found [41]. For FeSi doped with Co or Mn a T_C of about 60K has been observed. Hence the quest to find higher T_C doped semiconductors provides an incentive to study the isostructural CoSi and MnSi, and in particular their electronic properties.

In view of this, we have studied the formation of manganese silicide by deposition of the metal onto the silicon surface. This may produce various silicide phases depending on the film thickness and the annealing procedure like, for example, Mn_3Si, Mn_5Si_3, MnSi, $MnSi_2$ and $MnSi_{1.7}$. Among these, the most interesting phase from the point of view of the magnetic properties is bulk MnSi, which below 30K and at atmospheric pressure orders into a ferromagnetic state developing a long wavelength (180 Å) helical modulation in magnetic fields below 0.6T [42]. Also the Mn_5Si_3 phase has interesting magnetic properties: it has been observed that a transition between a non-collinear anti-ferromagnetism and a collinear ferromagnetism-paramagnetism occurs depending on the field applied and on the temperature [43].

The $MnSi_{1.7}$ phase is considered a promising thermoelectric material for high-temperature applications. It has been shown to grow epitaxially on silicon and could be used in optoelectronic applications such as silicon-based

infrared detectors and light sources [44]. $MnSi_{1.7}$ is a class of superstructures Mn_xSi_y where the ratio $\frac{x}{y}$ is ~ 1.7; this class is called "higher manganese silicide" (HMS). It seems that depending on the structure it may present either a direct bandgap near 0.7 eV [45] or an indirect gap near 0.4 eV [46]. The reason is that it may be either a continuum of ordered phases, or perhaps a group of several distinct compounds. The usefulness of such a semiconductor as an optoelectronic material depends on its growth mode and has led to a large amount of experimental studies.

4.2 Experimental set up

Photoemission and STM experiments were carried out in two different vacuum chambers. In the photoemission experiment, synchrotron radiation from the UE-56/2 beamline at the BESSY storage ring has been used, with the system equipped with a VG Scientific electron spectrometer. The UE-56/2 beamline provides for a very intense photon flux in the range of 60-1200 eV, giving the possibility to study both the VB and the core level electrons. The experimental total resolution was set to 100 meV for the Si $2p$ core level and to 250 meV for the valence band studies. The angular acceptance of the electron analyzer was 24°. All spectra were taken with an angle of incidence of 30° and at normal emission.

For the STM experiments, a home-built STM [47] was used, in a UHV chamber with a base pressure of 5×10^{-11} mbar with the STM operating at room temperature. Both UHV chambers are equipped with LEED for controlling and comparing the surface order.

The use of both STM and photoemission spectroscopy in the study of surfaces and thin films is due to the different information that can be obtained by the two techniques. While the former gives information about the local properties of the surfaces, the latter operates on a larger spatial scale depending on the photon spot incident on the sample and the analyzer aperture.

Due to the acceptance angle of the electron analyzer, photoemission is here used in such a way that the density of states (DOS) is measured and no angular information is possible. At a photon energy of about 65 eV, electrons escaping from the sample with an angle of 12° will have a corresponding wave vector of about 1 $Å^{-1}$ (see eq. 2.7), i.e. almost the width of the first

surface Brillouin zone.
As anticipated in chapter 2, photoemission from core levels permits to check the chemical composition of the sample and to study the charge transfer between atoms at different positions with respect to the surface and bound to species with different electronegativities. Thus, a detailed analysis of the core level line shape offers the possibility to study the effect of formation of the Mn/Si interface and to determine the formation of manganese silicide. The Si samples were cut from a commercial p-type Si(111) wafer (Virginia Semiconductors). To produce clean Si(111) surfaces, the samples were first degassed to $\sim$ 650°C for a few hours and then flashed at $\sim$ 1200°C. The pressure burst during the flash was maintained in the 10^{-10} mbar range. The samples were then quickly cooled to $\sim$ 900°C. The procedure ensured a good 7×7 reconstruction proved by the sharp 7×7 LEED pattern. Manganese deposition has been carried at room temperature from a water cooled Knudsen type MBE cell at a rate of 0.1 ML/min, where 1ML of manganese is defined as 7.88×10^{18} atoms/m^2.

4.3 Experimental results

The deposition of manganese in the initial stages and its effect on the surface symmetry has been characterized by means of LEED, where, in the range 1-5 ML, two distinct phases are found. While the LEED picture of 1 ML of Mn on Si shows a diffuse (1×1) phase with high background in which a faint (7×7) superstructure is still present (Fig. 4.1a), for more than 1.5 ML of manganese films annealed at 400°, a $(\sqrt{3}\times\sqrt{3})$R30° LEED pattern was observed, with no remaining substrate superstructure (Fig. 4.1c and d). The (1×1) spots become sharper after annealing at 250°C for 5 minutes, although very feeble remnant streaks of the (7×7) phase from the substrate are still visible (Fig. 4.1b). Any remaining doubt that the $(\sqrt{3}\times\sqrt{3})$ could be derived from the (1×1) structure is resolved by observing that the relative intensities of the (10) and (01) spots change in the two LEED patterns (*cf.* Fig. 4.1b and d). The existence of the above mentioned structural phases has been already reported by Evans [48], Nagao [49] and Kawamoto [50]. It has also been reported that up to 3 ML of Mn, deposited at RT at a slow rate of $<$ 0.15 ML/min, and annealed at 350°C, a sharp (1×1) LEED pattern is observed. However, as shown here, we found that the $(\sqrt{3}\times\sqrt{3})$

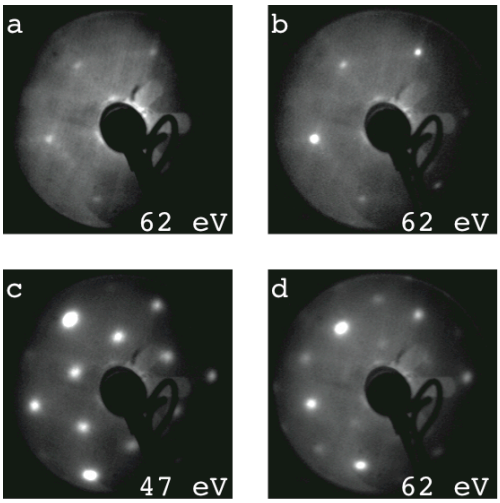

Figure 4.1: LEED images for (a) 1 ML Mn deposited on Si at room temperature, (b) same film as (a), annealed at about 250°C, (c) and (d) 2 ML Mn on Si annealed at about 400°C. The difference between (c) and (d) is only the electron energy.

reconstruction is already formed with 1.5 ML of Mn even with a lower deposition rate.

4.3.1 Morphology

Fig. 4.2 shows a STM image from a submonolayer Mn thin film on Si, after annealing at 250°C. Clusters of different sizes are present on the substrate, and the terraces of the silicon substrate, still distinguishable in this picture, are still very regular and have an average width of about 55 nm. Only about 1/3 of the largest clusters are formed on the terraces, while the steps are preferred, because of the necessity of incorporating Si atoms to form the silicide. In fact, when the clusters are formed on the terraces, they are surrounded by craters in the substrate, showing that silicide formation has already happened after a mild annealing, as expected from such reactive system.

The incorporation of silicon atoms into the deposited layer seems to be the path to form the silicide, with the consequent loss of order of the substrate surface. This becomes clearer in the close-up image of this layer in Fig.

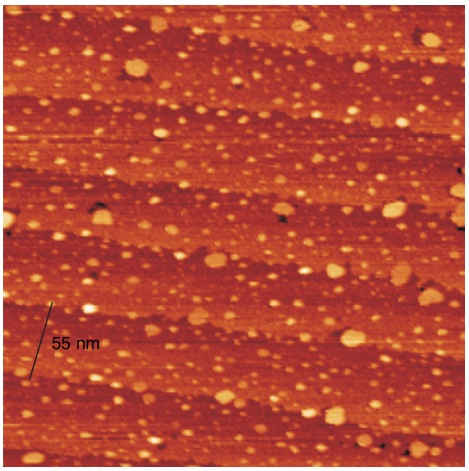

Figure 4.2: STM topography of about 0.5 ML Mn deposited on Si at RT and annealed at 250°C. The size of this image is 315×315 nm^2 and has been recorded at constant current I =1 nA, with sample bias voltage V_b = 1.7 V.

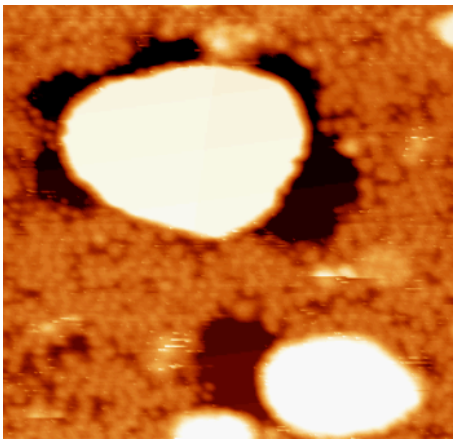

Figure 4.3: Atomic resolution STM image of clusters of different sizes. Some Si atoms from the substrate are incorporated in the clusters (dark holes in this image), while the others show disorder, with no trace of the (7×7) reconstruction. Image size is 27×27 nm^2. I =1 nA, with sample bias voltage V_b = 1.7 V.

4.3. The corresponding LEED image for this layer is Fig. 4.1a, with the streaks from the 7×7 Si reconstruction coming from the terrace region with no silicide clusters.

Increasing the manganese deposition to 2 ML and annealing this layer at 400°C, the reaction at the surface continues, destroying the terrace structure of silicon and making comparatively larger islands (see Fig. 4.4a). These are accommodated on patches of silicon substrate which are disordered and partially consumed by silicide formation. The growth of the silicide islands proceeds on the substrate in a Volmer-Weber mode [11], with the thin films covering the Si surface only partially. In the 3D image of another region

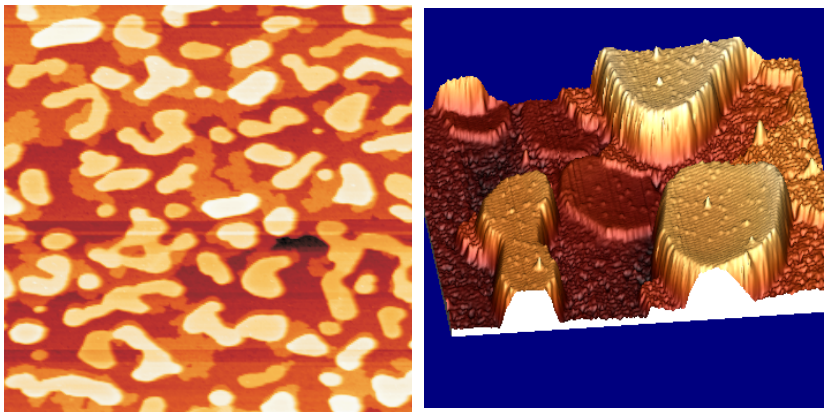

Figure 4.4: Deposition of about 2 ML Mn and annealing at about 400°C. (a) Substrate terraces are destroyed and elongated, flat islands cover partially the substrate surface. Image size is 315×315 nm^2. (b) 3D image of islands in the same sample as (a). Islands with different height lie on terraces of the Si substrate. Image size is 39×39 nm^2. I =1 nA, with sample bias voltage V_b = 1.7 V.

from the same sample, shown in Fig. 4.4(b), it is possible to see the silicide islands growing on the disordered silicon layer. The silicide islands have clearly different heights, varying, in this picture, between 1 and 3 ML. This confirms that the silicide formation takes place by incorporating silicon atoms into the deposited manganese layers.

The islands have a well-ordered atomic structure as evident from another closeup image in Fig. 4.5, of another sample obtained with a similar procedure. They exhibit perfect order in a $(\sqrt{3} \times \sqrt{3})$R30° arrangement with a number of additional "adatoms" in a three-fold coordination (Fig. 4.5).
The substrate also exhibits an atomically ordered surface structure with areas of Si(111)7×7 as well as of the metastable (5×5) reconstruction. This reordering of the substrate compared to the submonolayer deposition can be ascribed to the higher annealing temperature (400 °C) [49], which is close to the transition temperature where the (7×7) reconstruction forms from the metastable (2×1) phase on cleaved Si(111) [4].

By depositing more manganese onto the surface, the silicide islands start to coalesce, forming an almost closed film (Fig. 4.6), interrupted by deep holes. Nevertheless, most of the epitaxially grown surface area is flat with monatomic, 3 Å high islands on top (Fig. 4.7(a)), exhibiting a $(\sqrt{3} \times \sqrt{3})$R30° reconstructed surface as can be seen in Fig. 4.7(b).

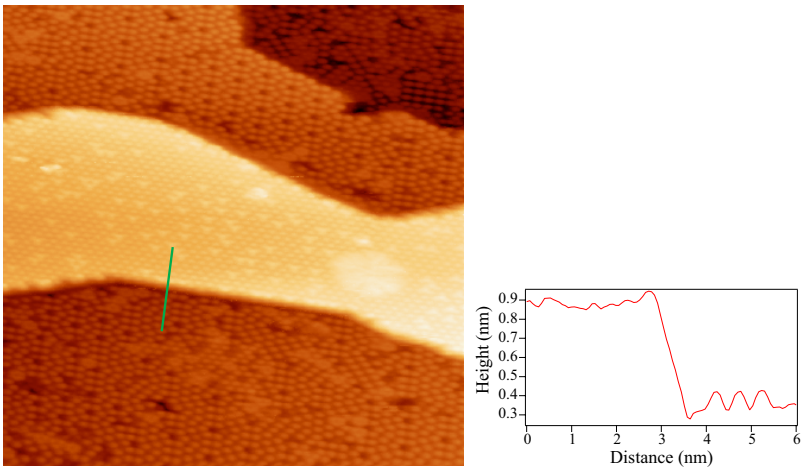

Figure 4.5: STM image of a silicide island and the Si substrate. The island has a $(\sqrt{3} \times \sqrt{3})$R30° order, with the presence of extra features due to adatoms. Also the substrate has various ordered regions, although with various atomic arrangements, varying from (7×7) to (5×5) and (9×9). The height of the large silicide stripe is about 6 Å, corresponding to 2 ML (left). The sample procedure is similar to that of Fig. 4.4, but with Mn deposition less than 2 ML. Image size is 34×34 nm^2. I =1 nA, with sample bias voltage V_b = 1.7 V.

The atomically resolved STM images of the silicide surface in the lower (1-2 ML) and in the higher (up to 5 ML) coverage regime reveal the frequent existence of adatoms which are three-fold coordinated and probably commensurate with the silicide crystal structure (Fig. 4.8(right)).
Moreover, by a more accurate observation of the STM images of the 5 ML Mn silicide (cf. Fig. 4.6 and Fig. 4.8(left)), it is possible to note that, although most of the surface area is flat, large scale modulations in STM with a period of about 20 nm are present. These exhibit a hexagonal symmetry pattern which suggests that the modulation can be ascribed to the formation of a strain network in the silicide film due to a mismatch in the epitaxial growth of the silicide onto the silicon substrate. This modulation is an example of a Moiré pattern which is obtained by superimposing two crystals with a small mismatch and with some degree of displacement [51].
The nature of the deep holes that can be found besides the flats is also interesting. The depth of these holes can be as much as 30 Å. On the bottom, the holes consist of unreacted silicon as can be seen from the residual reconstruction patterns (Fig. 4.9). The holes are thought to act as local relief

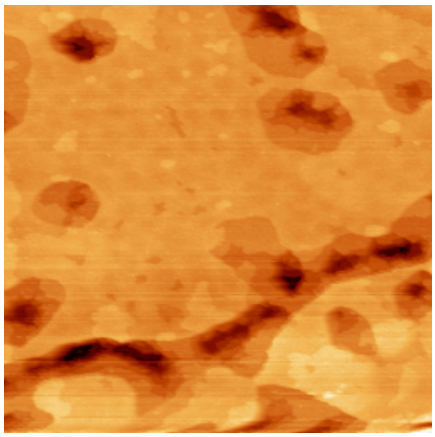

Figure 4.6: STM image of 5 ML Mn deposition and annealing at about 400°C. The film is flat and covers almost completely the substrate, although holes are still present. Image size is 315×315 nm^2. I =1 nA, with sample bias voltage V_b = 2 V.

to the strain due to lattice mismatch, as suggested by the presence of the Moiré pattern.

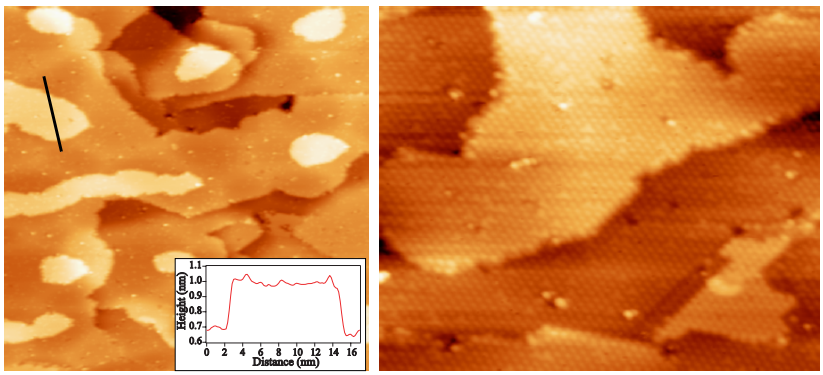

Figure 4.7: STM image of 5 ML Mn deposition and annealing at about 400°C. Flat islands grow on top the thin film (left), showing ($\sqrt{3} \times \sqrt{3}$)R30° reconstruction (right). Islands are about 3 Å high. Image sizes are 85×85 nm^2 and 29×29 nm^2, respectively. I =1 nA, with sample bias voltage V_b = 1.7 V.

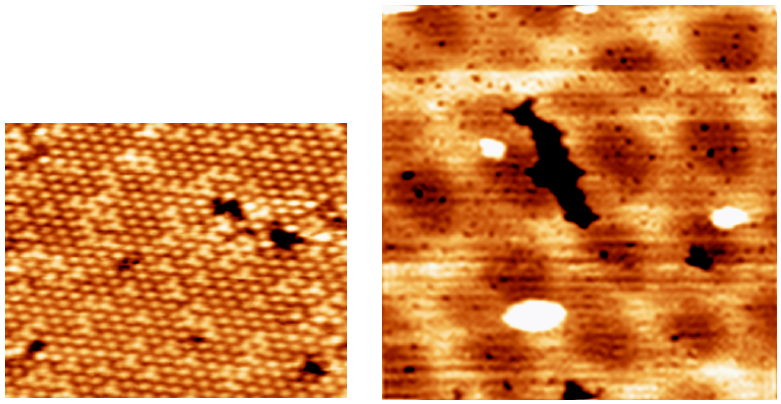

Figure 4.8: (left) The $\sqrt{3}\times\sqrt{3}$)R30° reconstructed surface has many defects and three-fold coordinated adatoms. (right) The STM contours show modulations with an approximately hexagonal symmetry. The period of the network is of the order of 20 nm. The surface shows also a high density of defects and eventually deep holes. Image size is 16×14 nm^2 (left), and 86×86 (right). I =1 nA, with sample bias voltage V_b = 1.7 V (left) and 2 V (right).

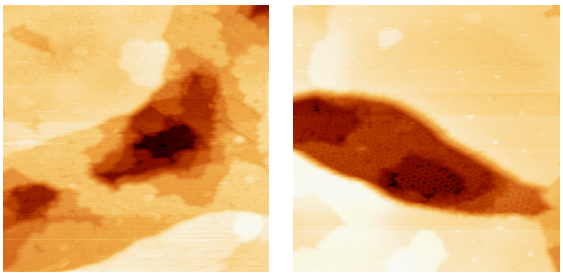

Figure 4.9: Several layer deep holes are present also in the 5 ML film. It never covers the surface completely because the silicide film is strained, due to a lattice mismatch with the silicon substrate. At the bottom of 30 Å deep holes, unreacted silicon is still present (left). Image size is 58×58 nm^2 and 48×48 nm^2, respectively. I =1 nA, with sample bias voltage V_b = 1.7 V.

4.3.2 Spectroscopy

STM topography reveals the growth mode *via* island formation and the morphology of the reacted films. However, to obtain information about the electronic properties of these films, this system has been studied also by photoemission. The results can be sorted into two different classes: from the angle integrated normal emission valence band spectra, it is possible to

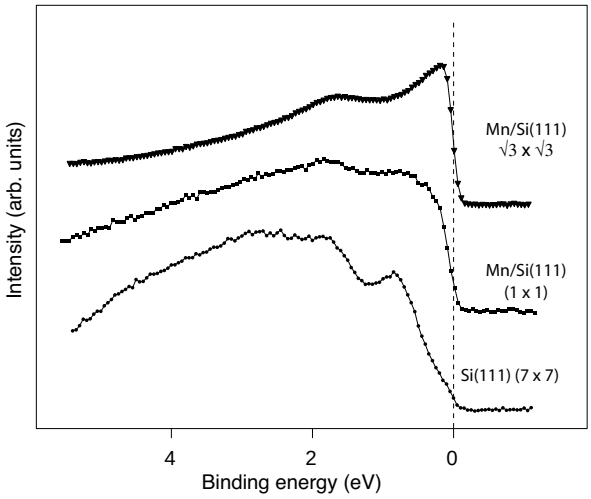

Figure 4.10: Valence band photoemission spectra taken with a photon energy of 65 eV for the (1×1) and the $(\sqrt{3} \times \sqrt{3})$R30° phases obtained by annealing 1 ML and 2 ML of Mn epitaxial films on Si.

observe the difference in electronic character of the various phases inferring which particular silicide corresponds to the actual phase, while with core level spectroscopy, information about the charge transfer between silicon and manganese atoms and the composition of the silicide surface have been obtained.

Valence band spectra have been recorded with a photon energy of 65 eV. In Fig. 4.10, photoemission spectra of the clean Si(111)7×7, the Mn/Si(111)-(1×1) and the Mn/Si(111)$(\sqrt{3} \times \sqrt{3})$R30° surfaces are shown. The valence band spectrum for clean Si(111)7×7 is characterized by three features next to the Fermi edge, corresponding to the three surface states at 0.2, 0.8 and 1.8 eV binding energy, which have been attributed to ad-atoms, rest atoms and back bonded atoms, respectively [52]. These peaks are very sensitive to the deposition of manganese. Just one ML of Mn is sufficient to destroy the surface states of Si(111)7×7, as is clear from the valence band spectrum relative to the (1×1) phase, where two very broad features at ∼1.0 eV and ∼2.0 eV are present and, at the Fermi level, the photoemission intensity is very low. The feature at 1.0 eV is derived from Mn 3*d* non-bonding states while the one at 2.0 eV is from the bonding Mn 3*d* - Si 3*p* states [34]. Taking into account the overall energy resolution of our spectrometer, the decreasing

photoemission signal is interpreted as a signature of the semiconducting character of the (1×1) reconstructed surface.

Very different from the (1×1) phase is the valence band spectrum from the $(\sqrt{3} \times \sqrt{3})$R30° surface. In fact, in this case, a sharp Fermi edge is observed, which demonstrates the metallic character of this surface in agreement with STS results. The corresponding valence band spectrum is presented in Fig. 4.10(top), where a $(\sqrt{3} \times \sqrt{3})$R30° LEED pattern is obtained by depositing 2 ML of manganese on Si and annealing at 400°C, but it does not change with further Mn deposition. The bulk silicides which have metallic character are MnSi and Mn_5Si_3, therefore it is possible to determine which particular phase is obtained by comparing the data present in the literature concerned with these two components.

In the experimental valence band spectrum of Mn_5Si_3, a sharp peak, close to E_F, and two broad peaks at 1.3 and 3.0 eV are observed [43], whereas a sharp peak close to E_F and a weak feature at ∼2 eV have been reported for MnSi [53]. Thus, by comparing the valence band spectrum of the $(\sqrt{3} \times \sqrt{3})$R30° - phase with one of the known bulk metallic phases as well as with the band structure calculations of the known bulk phases of manganese silicides [54], we believe that the electronic structure of this phase is similar to that of bulk MnSi.
Such an inference is in agreement with the findings of Nagao *et al.* [49], who, from their scanning tunneling microscopy measurements, also concluded that in the $(\sqrt{3} \times \sqrt{3})$R30° -phase, the ratio between Si and Mn atoms is 1:1. Therefore, in agreement with the band structure calculations for MnSi, we assign the feature close to E_F to Mn 3*d* states and the feature at 1.7 eV to Mn 3*d* - Si 3*sp* derived bonding states.

Si 2*p* core level spectra of Si(111)-(7×7), with 1 ML and 2 ML of Mn overlayers as-deposited and the (1×1) and $(\sqrt{3} \times \sqrt{3})$R30°-phases, obtained by annealing these thin films, are shown in Fig. 4.11. All spectra were recorded with a photon energy of 150 eV, which assures a good surface sensitivity for the 2*p* core-level. As is obvious from the core level spectrum of an as-deposited 1 ML thin film of Mn, all features due to surface components [55], which are clearly visible in the core-level spectrum of Si(111)-(7×7), almost disappear.
The main peak is shifted by about 80 meV towards lower binding energy in comparison to the Si 2*p* main peak of Si(111)-(7×7) and has a weak shoulder

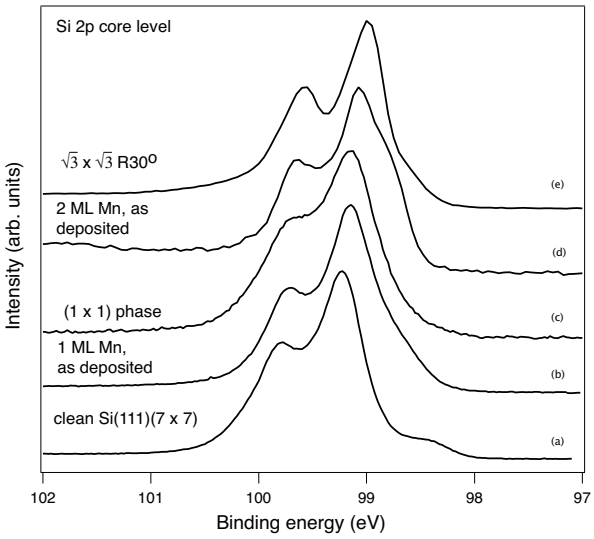

Figure 4.11: Si 2p core level spectra obtained with a photon energy of 150 eV for (a) Si(111)-7×7, (b) and (d) as-deposited Mn epitaxial films of 1ML and 2ML thickness, respectively, (c) the (1×1) phase and (e) the $(\sqrt{3} \times \sqrt{3})$R30° phase.

at ∼-0.3 eV binding energy with respect to the main peak. It is therefore clear that the metal-silicon reaction occurs already at room temperature, and that it results in the formation of Mn silicide on the Si surface.
On annealing the film to 200°C to obtain the (1×1)-phase, no big changes are observed, only a further chemical shift of about 20 meV and a small decrease in the peak-to-valley ratio of the Si 2p doublet of the main peak. At 2 ML of Mn the line shape changes, indicating an increase in the intensity of the reacted component with the result of a shift of the main peak increased to about 150 meV.
For the $(\sqrt{3} \times \sqrt{3})$R30°-phase, the main peak is shifted by -0.23 eV and is comparatively narrower. Further, it also exhibits a shoulder at ∼-0.5 eV, which is very similar to the S_2 surface component of Si(111)-(7×7). This suggests that the surface of this phase is terminated by Si atoms.

Apart from these first observations, more information can be obtained by exploring the contributions of various components to the Si 2p core-levels, analysing the spectra by means of a least squares fitting.
To model the photoemission lines we used Lorentzian peaks numerically convoluted by a Gaussian (for the description of instrumental and phonon

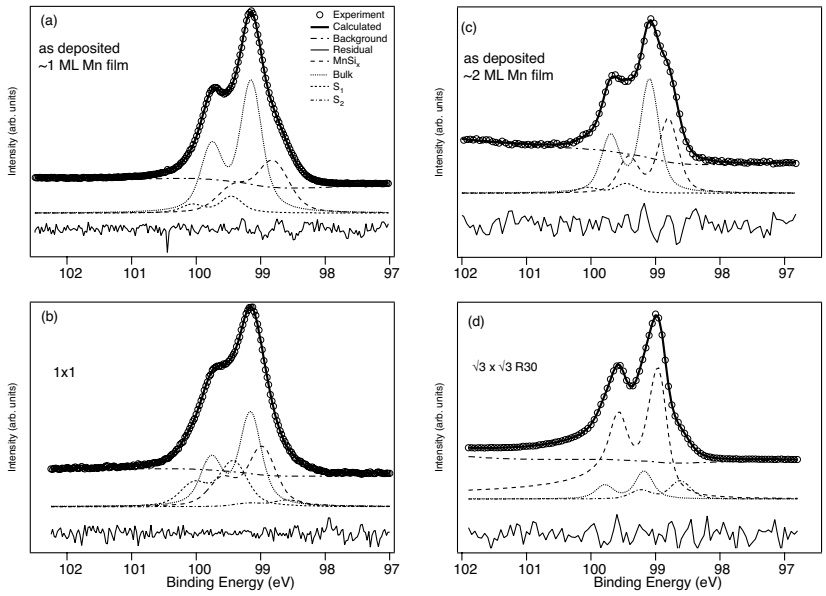

Figure 4.12: The best fit spectra for Si 2p core levels recorded with photon energy of 150 eV for (a) as-deposited Mn epitaxial film of 1 ML Mn on Si(111)-(7×7), (b) 1×1-phase, (c) as-deposited 2 ML Mn on Si(111)-(7×7) and (d) $(\sqrt{3}\times\sqrt{3})$R30° phase. The experimental data are represented by open circles, while the fits to the data are given by the thick solid line; the contribution of various components to the respective Si 2p core levels are displayed underneath each spectrum.

broadening and surface disorder), as in the case of the SiC core level shifts in chapter 3.

The Si 2p spectrum for clean Si was fitted (not shown) in terms of known surface and bulk components and the parameters obtained were found to be consistent with the earlier published results [55]. In each of the Si 2p core-levels, all the Si 2p doublets representing contributions from different environments of Si atoms are well described by a spin-orbit splitting of 0.608±0.003 eV and a Lorentzian width of 0.070±0.020 eV.

The Si 2p core-level for the as-deposited 1 ML of Mn film is well described in terms of three components (Fig. 4.12a), with the main component at 99.15 eV binding energy and the other two having a chemical shift of 0.28 eV and -0.34 eV. Taking into account the relative binding energies of different bulk and surface contributions to Si 2p core-level of Si(111)7×7, we assign the component at 99.15 eV binding energy to emission from bulk Si atoms. The

second one at higher binding energy to the S_1 surface component represents the back-bonded atoms from the Si substrate.

The third component at lower binding energy then can be ascribed to the silicide phase formed due to reaction between the Mn atoms from the thin film and Si atoms from the substrate. It may be noted here that in comparison to clean Si, relatively large Gaussian widths were found from the fitting procedure, implying that the interface is characterized by large disorder as would be expected for an as-deposited film and as observed in STM.

One of the main reasons for the observed large disorder for the reacted component (manganese silicide, $MnSi_x$) could be due to the fact that the reaction between Mn and Si is not complete and $MnSi_x$ exists with different values of x, leading to a large variety of nearest neighbour environments for the Si atoms. The contribution of large intensities from the substrate confirms that deposition of 1 ML of Mn does not lead to a uniform coverage of the complete substrate surface, which implies that during the initial stages of growth, island formation instead of uniform film takes place, in agreement with our result from the STM experiment.

In case of the Si $2p$ core level for the 1×1-phase (Fig. 4.12b), obtained by annealing the 1 ML Mn film at 250°C for 5 minutes, the introduction of an extra component shifted by 0.58 eV with respect to the bulk Si contributions was found to be necessary to arrive at a good description of the line shape. This component has been ascribed as S_2, due to emission from the adatoms. Further, a decrease in the intensity of bulk component and increase in the intensities of the $MnSi_x$ and S_1 components with a concomitant decrease in the Gaussian widths of all the three components is apparent from the figure. On annealing the 1 ML Mn film, the reaction between the Mn and Si atoms proceeds further, possibly leading to the formation of single phase $MnSi_x$, and the bare areas of the substrate between the silicide clusters become more ordered.

The increase in the intensity of S_1 and reappearance of S_2 surface components would also imply that at least in some of these bare areas, the formation of the (7×7) superstructure has recurred, which may not have a completely perfect dimer-adatom-stacking fault (DAS) structure, as confirmed by the observation of feeble streaks of (7×7) in LEED pattern of this phase (Fig. 4.1b). The surface core-level, S_2 in Si(111)-(7×7) is shifted by about 0.70 eV [55], while in the (1×1)-phase the shift has been found to be

0.58 eV with a relatively larger Gaussian width. This leads us to believe that the S_2 component not only has the contributions from the (7×7) superstructure of the bare substrate, but the surface of the 1×1-phase is also terminated by Si atoms.

For the as-deposited ∼2 ML Mn thin film, the Si 2*p* core-level is well described in terms of three components, identified as contributions from the bulk and back-bonded atoms of the substrate and the manganese silicide phase (Fig. 4.12c). As in the case of an as-deposited 1 ML Mn film, here also a large intensity for the contributions from bulk Si-atoms and back-bonded atoms of the substrate is observed, indicating that even after deposition of 2 ML of Mn, the film is not completely closed. This supports our earlier inference that the growth of Mn on Si(111)7×7 takes place by formation of islands, which is in agreement with the earlier STM findings [48],[49].
The Si 2*p* core-level for the $(\sqrt{3} \times \sqrt{3})$R30°-phase (Fig. 4.12d) is mostly dominated by a single peak attributed to the silicide phase, which is possibly MnSi, as observed above for the valence band spectrum. Apart from this, relatively small contributions from the Si bulk atoms and adatoms are also clearly evident from the figure.
The occurrence, in the Si 2*p* core-level of this phase, of one component with high intensity, attributed to the reacted silicide MnSi, suggests that the annealing of the film at 350°C leads to completion of the reaction between Mn and Si, resulting in the formation of the silicide with almost complete coverage of the Si substrate. Nevertheless, the presence of some bare areas of the substrate, observed in STM also for films 5 ML thick, is also revealed in the core level PE spectrum of Fig. 4.12d, by the presence of the S_1 component, although its intensity is only 1/4 of the MnSi peak.
It has to be noted here that to arrive at a good agreement with the experimental Si 2*p* line shape for the $(\sqrt{3} \times \sqrt{3})$R30°-phase, it was found to be necessary to describe the line shape of the MnSi component by a Doniach-Sunjic function [56], instead of a Lorentz function. This is not completely surprising considering the fact that MnSi is metallic. Similar results were obtained from the analysis of Si 2*p* line shape for the $(\sqrt{3} \times \sqrt{3})$R30°-phase obtained from the 5 ML of Mn film.

The observation of a component similar to the S_2 surface core level of Si(111)-(7×7) in the Si 2*p* core levels of (1×1) and $(\sqrt{3} \times \sqrt{3})$R30° surface

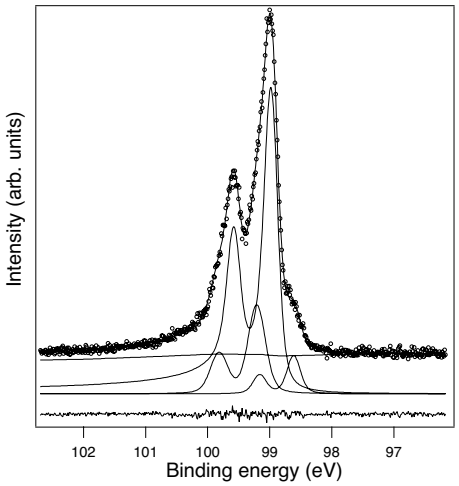

Figure 4.13: $(\sqrt{3} \times \sqrt{3})$R30°-phase recorded with a photon energy of 120 eV, with the corresponding line shape analysis shown underneath.

reconstructions is puzzling if not completely surprising. In a recent study, Ctistis *et al.* [57] in their RHEED studies on thin films of Mn on Si(111)-$(\sqrt{3} \times \sqrt{3})$:Bi observed that annealing of such films at 250°C results in ordered films with a Si layer on top of the Mn film. Similarly, the annealing of epitaxial Ni films on Si(111)-(2×1), have also been reported [58] to be accompanied with out-diffusion of silicon atoms having epitaxial arrangement of the silicide surface. More recently, in a theoretical work [59], Wu *et al.* predicted that ultrathin Si-Mn sandwich films grown pseudomorphically on Si(001) are obtained by a diffusion of a single Mn atom into a second layer interstitial site below the Si dimer, and present ferromagnetic character.
In order to explicitly check that this component originates from the Si atoms on the surface of the silicide and not from the bare areas of the substrate, we recorded Si 2*p* core level PE spectra for the $(\sqrt{3} \times \sqrt{3})$R30°-phase with a photon energy of 120 eV, thus increasing the escape depth of the electrons. The corresponding spectrum is shown in Fig. 4.13. Even without any detailed line shape analysis, it is evident from the experimental spectrum that the intensity of the leading clean Si peak is markedly decreased compared to the surface sensitive spectrum at 150 eV photon energy. Specifically, the results of the line shape analysis indicate that there is an attenuation of 30% in intensity of this component thus clearly proving that this component in-

deed originates from emission from Si atoms on the surface of MnSi. Since in the LEED pattern, only the $(\sqrt{3} \times \sqrt{3})$R30° structure is observed, we believe that the atomic structure of these surface Si atoms is commensurate with the $(\sqrt{3} \times \sqrt{3})$R30°-phase of MnSi.

4.4 Conclusions

The deposition and reaction of ultrathin Mn films on Si-(7×7) were studied by means of LEED, STM and photoemission spectroscopy. While the reaction between Mn and Si begins already at RT leading to an incomplete silicide formation, annealing these Mn films results in the development of well ordered manganese silicide phases. At very low coverages, of less than about 1 ML of Mn, the development of silicide islands is observed in STM images resulting in a (1×1) LEED pattern. The valence band photoemission spectrum indicates that this film is semiconducting. At higher Mn coverages, up to 5 Ml, a $(\sqrt{3} \times \sqrt{3})$R30° phase develops, as shown by LEED, in a Volmer-Weber mode, with islands interrupted by bare Si substrate patches at low coverages and the film being nearly closed at 5 ML. In this coverages range, a strain dislocation network is manifested as a large scale corrugation seen in STM. Photoemission experiments attributed these films to the metallic MnSi phase, terminated with Si adatoms.